

Concerns about Modelling of Foregrounds and the 21-cm Signal in EDGES data

RICHARD HILLS,¹ GIRISH KULKARNI,^{2,3} P. DANIEL MEERBURG,^{2,3,4,5,6} AND
EWALD PUCHWEIN^{2,3}

¹*Astrophysics Group, Cavendish Laboratory, J. J. Thomson Avenue, Cambridge CB3 0HE, UK;
richard@mrao.cam.ac.uk*

²*Institute of Astronomy, University of Cambridge, Madingley Road, Cambridge CB3 0HA, UK*

³*Kavli Institute of Cosmology, University of Cambridge, Madingley Road, Cambridge CB3 0HA, UK*

⁴*DAMTP, Centre for Mathematical Sciences, Wilberforce Road, Cambridge CB3 0WA, UK*

⁵*Kapteyn Astronomical Institute, University of Groningen, P. O. Box 800, 9700 AV Groningen,
The Netherlands*

⁶*Van Swinderen Institute for Particle Physics and Gravity, University of Groningen, Nijenborgh 4,
9747 AG Groningen, The Netherlands*

ABSTRACT

We have re-analyzed the data in which [Bowman et al. \(2018\)](#) identified a feature that could be due to cosmological 21-cm line absorption in the intergalactic medium at redshift $z \sim 17$. If we use exactly their procedures then we find almost identical results, but the fits imply either non-physical properties for the ionosphere or unexpected structure in the spectrum of foreground emission (or both). Furthermore we find that making reasonable changes to the analysis process, e.g., altering the description of the foregrounds or changing the range of frequencies included in the analysis, gives markedly different results for the properties of the absorption profile. We can in fact get what appears to be a satisfactory fit to the data without any absorption feature if there is a periodic feature with an amplitude of ~ 0.05 K present in the data. We believe that this calls into question the interpretation of these data as an unambiguous detection of the cosmological 21-cm absorption signature.

1. ANALYSIS

The recent detection by [Bowman et al. \(2018\)](#) of an absorption profile at ~ 78 MHz in the sky spectrum, averaged over a wide range of angles, has excited much interest. It is suggested that this is due to absorption by the 21-cm line of atomic hydrogen that arises from the effects of the light from the first stars falling on the gas. If this is the cause, then both the large depth, ~ 0.5 K, and the flat-bottomed shape are unexpected. The detection of such a weak feature is extremely challenging because of the strong foreground radiation, mostly due to Galactic synchrotron emission, which is >1000 K at these wavelengths. In the methods section attached to their Letter, [Bowman et al. \(2018\)](#) describe the great care that was taken in the design and execution of the EDGES experiment to obtain accurate measurements of the sky temperature and to ensure that the “signature” is global, e.g., that it does not vary significantly with the position of the Galactic plane in the sky. They also

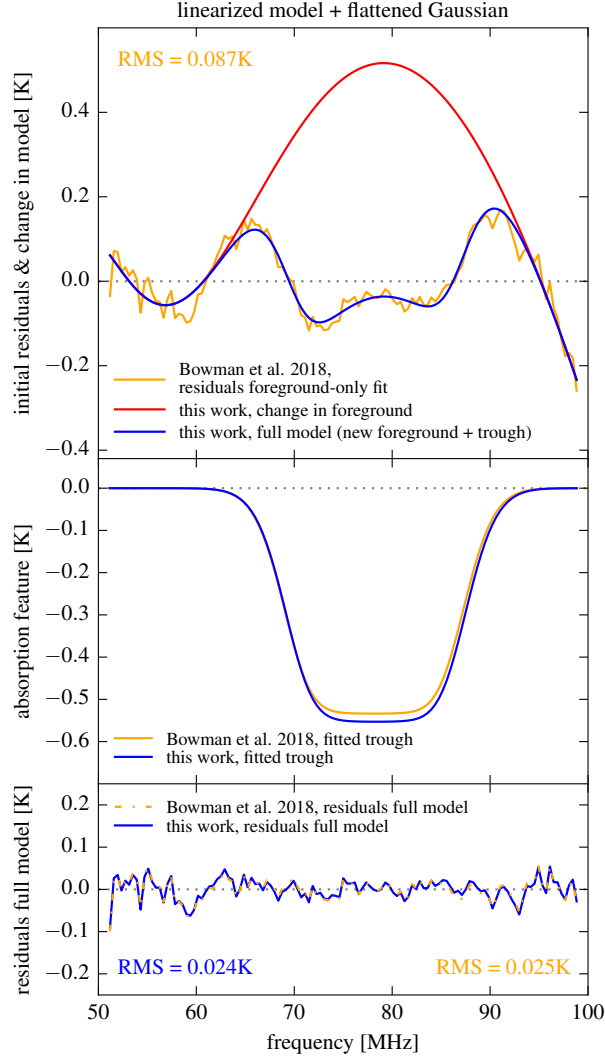


Figure 1. Fits to the EDGES data (cf. Figure 1 of Bowman et al. 2018). The top panel shows the residuals obtained by Bowman et al. 2018 with the linearized foreground model alone. We get almost identical residuals (~ 0.0015 K rms difference, not shown for clarity) when fitting the same model. Adding the flattened Gaussian profile to the model reduces the residuals, as seen in the bottom panel, but this requires a modification to the foreground model that is much larger than the initial residuals, as is shown by the red curve in the top panel. The blue curve in the top panel illustrates how the full model approximates the residuals. The residuals of the full model are again almost identical to those in the release and the parameters for the absorption profile (middle panel) are very close to those given by Bowman et al. 2018.

give details of the methods that they used to separate the foreground emission from the apparent absorption profile, but they do not discuss the interpretation of foreground fits, nor do they give quantitative results from this fitting. Here we revisit the analysis¹ focusing on the interpretation of the foregrounds.

¹ We use the data available at <http://loco.lab.asu.edu/edges/edges-data-release/> throughout our analysis.

The first step, that of confirming that we are performing the same analysis, is illustrated in Figure 1. Here the fitting functions were as described by Bowman et al. (2018), where the foreground is the linearized version of a physically-motivated model, which has 5 free parameters (see Equation 8)², and the absorption profile is a flattened Gaussian, which contains a further 4 free parameters (see Equation 2). In the figure we show how the change in the fitted foreground (top panel, red curve) and the absorption profile (middle panel, blue curve) combine to make the blue curve in the top panel, which shows how the model with the profile approximates the initial residuals. It is only the presence of the ~ 0.5 K peak change to the foreground model that converts the two positive features seen in the residuals in the top panel into the deep feature which is being interpreted as an absorption profile.

A general concern is that a total of 9 parameters are being adjusted to achieve a fit to data which span ~ 50 MHz and where the structures apparent above the noise seem to have characteristic widths of ~ 5 MHz or more. This makes it essential to examine the values of all the parameters resulting from the fits. We feel that to focus so much attention on the 4 values describing the absorption profile, but then to neglect discussion of the remaining 5 parameters, as Bowman et al. (2018) appear to have done, risks missing important clues in the interpretation of the data. The values for the parameters that we find for all the cases that we have considered are given in Table 1. For the case shown in Figure 1 we find that first and fifth parameters describing the foreground, which should represent, respectively, the bulk of the synchrotron emission from the Galaxy and the emission from electrons in the ionosphere at 75 MHz, have values of $\sim -15,400$ K and $\sim 17,000$ K, respectively, for the fit without the absorption profile, and $\sim -10,100$ K and $\sim 11,700$ K with the absorption profile. Clearly these cannot be given a meaningful physical interpretation, but the large values with opposite signs indicate that the parameters are very highly correlated and the large changes when the profile is added to the model indicate that they are strongly coupled to those parameters as well.

Bowman et al. (2018) also give the expression for the physically-motivated foreground model from which the linearized version is derived. Using this non-linear model should provide more insight into the interpretation of the data. We performed such fits using both least-squares and Bayesian sampling, which can show the correlations and the ranges of acceptable values for the parameters. (See Supplementary Information for details.) We find that a good fit is only obtained when the term representing the optical depth of the ionosphere is negative, which is clearly non-physical, and the emission from the ionosphere is about half of the total, which again cannot be correct at these wavelengths (Evans and Hagfors 1968). In reality the ionospheric absorption and emission should be linked via the effective temperature of the electrons, T_e , since the emission is expected to be thermal. We included this coupling explicitly and did the analysis again, restraining the parameters so that the opacity at 75 MHz could not be less than 5 parts per thousand (Rogers et al.

² All equations, a table of parameter values, and additional figures are in the Supplementary Information in Section 4.

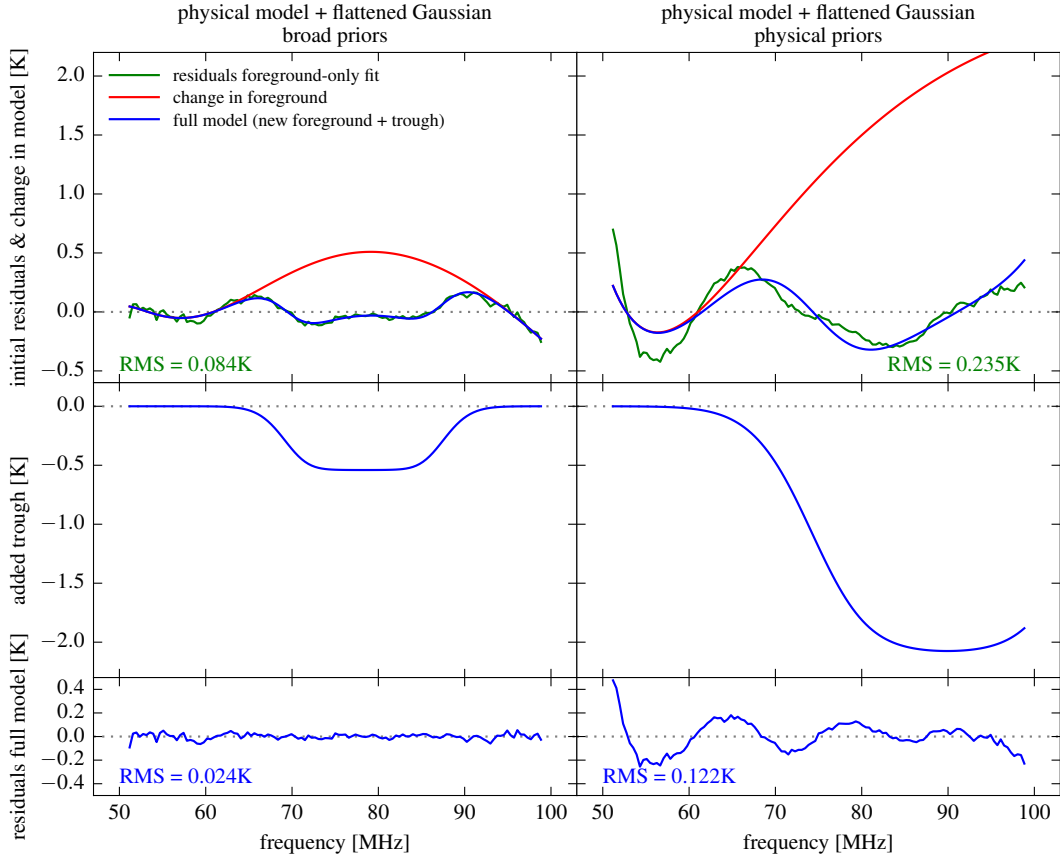


Figure 2. Panels in the left column show results when the foreground parameters are left free to assume any value. Panels in the right column show results when these parameters are constrained to take physically plausible values. As no good least-square fit is obtained in the latter case, the mean value of the parameters from the posterior of the Bayesian analysis were adopted.

2015) and T_e was in the range 200 to 2000 K. We also restricted the centre frequency of the absorption profile to be in the range 60 to 90 MHz. The results obtained for these two cases, with and without the restrictions on the parameters, are shown in Figure 2. It is seen that without the restrictions a good fit is obtained, with essentially the same profile and residuals as with the linearized model, but that with the restrictions the fit is poor, the centre of the profile has moved to the upper limit and it now has a depth of ~ 2 K. The corresponding residual rms is 0.122 K.

As an alternative approach to trying to attach a physical significance to the parameters describing the foregrounds, one can simply assume that the foregrounds must be smooth in character and that what we are looking for are features that cannot be fit by a smooth profile. Bowman et al. (2018) also considered this approach and adopted a polynomial form for the foreground with terms in frequency raised to the power -2.5 , -1.5 , etc. When we use this model we find that there is substantial ambiguity in the parameters for the absorption profile. This is illustrated in Figure 3. If we use 5 terms in the polynomial, and fit for the absorption profile using all of the data, which covers the range from 51 to 99 MHz, we find

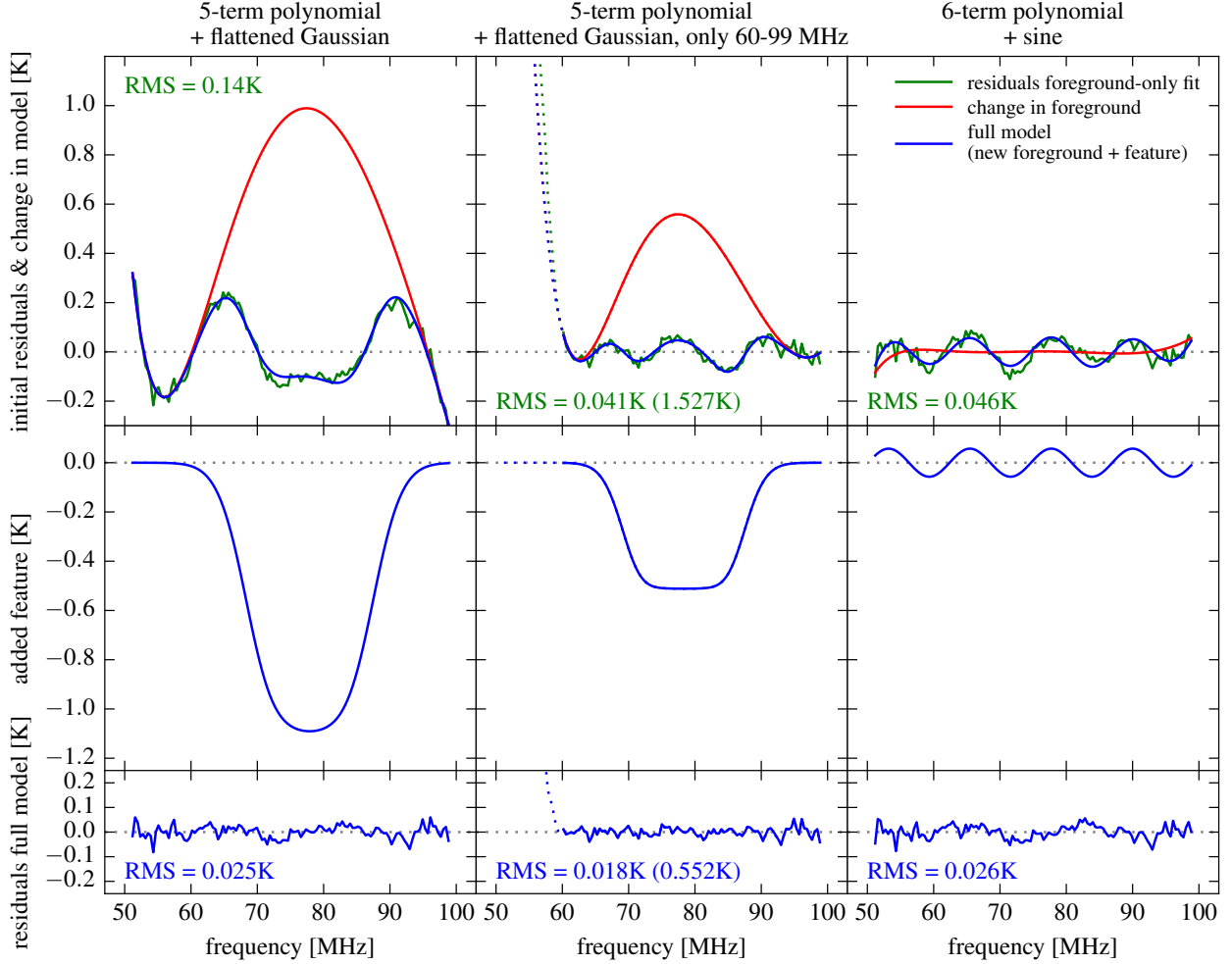


Figure 3. Fit and residuals using a polynomial foreground model with the full data set (left column), using only a restricted range of frequencies (middle column), and using the full data set but with a sine wave instead of the flattened Gaussian profile (right column). The rms values in brackets in the top and bottom panels in the middle column are for the full data set.

an absorption feature which has an amplitude of ~ 1 K and is much less flattened than that reported by [Bowman et al. \(2018\)](#). This is shown in the left column of Figure 3. The residuals for this fit have an rms of 0.025 K, i.e., the fit is just as good as that obtained with the physically-motivated model and with the same number of free parameters (9), but the absorption feature found has very different properties. Bayesian analysis again confirms this ambiguity, see Figure 7.

When using this polynomial foreground model, [Bowman et al. \(2018\)](#) generally only made the fit to the data over a restricted frequency range. When we use just the range 60–99 MHz, we do recover the flattened feature with ~ 0.5 K amplitude (middle column of Figure 3). The residuals in the region below 60 MHz are however then very large, reaching ~ 3 K at 51 MHz. It is not clear what justification there is for ignoring the data in the range 50–59 MHz when using this description of the foregrounds. It is also notable that the residuals from the 5-

term polynomial fit made without the absorption feature (middle panel top row of Figure 3) show an undulating feature. It is clear that it is again the combination of the change in the background (red curve) and the flattened Gaussian profile that is being used to remove these undulations and give a good fit. If we increase the number of terms in the polynomial to 6 and use the data covering the whole frequency range, the residuals (top right in Figure 3) again show the undulating feature. A good fit can, in this case, be obtained by using a sine wave instead of the flattened Gaussian. The period found is ~ 12 MHz and the amplitude is only ~ 0.05 K in contrast to the ~ 0.5 K depth found using the flattened Gaussian profile. The residuals are similar in magnitude and the total number of free parameters is again 9. It is not clear how much significance should be attached to this result, but it is worth noting that undulations with similar periods appear in Extended Data Figure 4(c) of [Bowman et al. \(2018\)](#) in the context of “chromaticity” (frequency dependence) in the antenna gain.

2. DISCUSSION

It is important to ask whether it should be necessary to use so many terms to describe the synchrotron emission from the Galaxy and other sources and to take account of the effects of the ionosphere. This question was addressed by [Bernardi et al. \(2015\)](#), who showed that, while 5 or even 6 terms might be needed to describe the synchrotron foreground in what they describe as a pathological case, 3 terms should be sufficient over the 50 to 100 MHz range when a more realistic model of cosmic ray diffusion is used. The frequency dependence of the emission and absorption due to the ionosphere should be well described by a simple model (see Equation 1) and in principle this can be accounted for by applying a correction to the data based on the density and temperature of the ionosphere at the time of observation, instead of allowing the ionospheric effects to be free parameters in the fits.

It appears to us that the process of fitting the data with many parameters and then focusing on the residuals can be misleading. It is important to ask what signature can be seen in the data before performing any fits. Because of the very steep variation in the sky temperature with frequency, it is not easy to present the data in a way that provides insight—even a log-log plot looks like a straight line. Taking the logarithmic³ derivative $d(\log T)/d(\log \nu)$ provides a measure of the apparent change in the spectral index as a function of frequency and we find this to be revealing.

The upper panel of Figure 4 shows the result of logarithmic differentiation of the data. The blue curve shows the result when no correction for the ionosphere has been applied. The various fits described above have, in essence, been trying to reproduce the curved shape seen in this plot. It seems likely that this curvature is associated with the non-physical values found for the parameters.

The ionospheric emission and absorption does have a significant effect on the apparent spectral index. To show this we have applied corrections to the data (by inverting Equation 1) assuming a simple uniform slab model for the ionosphere with a temperature of 800 K

³ ‘log’ denotes the natural logarithm throughout.

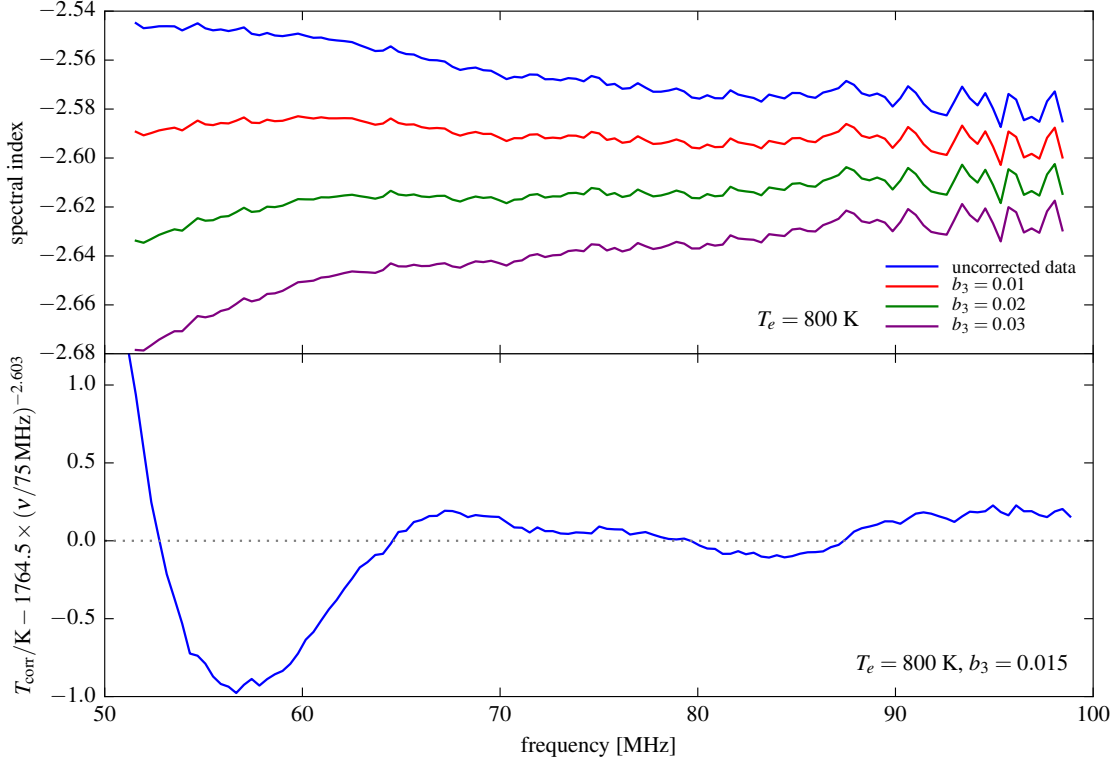


Figure 4. Top panel: Running of the spectral index of the EDGES data (blue curve). The other curves in this panel show the same quantity after correcting for different assumed values of the ionospheric opacity. Bottom panel: Sky temperature corrected for ionospheric opacity, assuming $b_3 = 0.015$, after subtraction of a simple power-law model. All curves in the figure assume an electron temperature of 800 K.

(Rogers et al. 2015) and opacities at 75 MHz of between 10 and 30 parts per thousand. The ionospheric opacity is the parameter b_3 in the notation of Equation (6). We understand (Rogers, private communication) that the mean opacity at the times when these data were taken is likely to have been in this range. It can be seen that with opacities between $b_3 \sim 0.01$ and $b_3 \sim 0.02$ the spectral index is nearly flat over much of the band, but that it appears to steepen (become more negative) at the low-frequency end. The value of the spectral index in the flat part ($\nu \gtrsim 65$ MHz) agrees well with the determination by Mozdzen et al. (2016) for EDGES in the 90–190 MHz range.

In the lower panel of Figure 4 we show the residuals after correcting for the ionosphere using a value of $b_3 = 0.015$ and then subtracting a “minimal” foreground model, which is just a power-law with a fixed spectral index. Whereas the plots in the upper panel make no assumptions at all about the nature of the spectrum, the appearance of the lower plot is somewhat subjective in that we have chosen the ionospheric opacity and the magnitude and spectral index of the foreground in order to reduce the dynamic range of the data in the plot: effectively we are doing a three-parameter fit. (The assumed electron temperature has very little effect on the appearance of this plot.) We nevertheless feel that this gives a good qualitative impression of the features in the data which need to be explained as

being of either instrumental or astronomical origin. We suggest that examining in these ways the various subsets of data taken at different Galactic Hour Angle and with different experimental setups may be helpful.

The features seen in Figure 4 and the non-physical values of the parameters found in the fits suggest that, instead of interpreting the values as being exact measurements of the sky-averaged temperature, which is what we have done so far, we need to consider the possibility that there are residual systematic errors. [Bowman et al. \(2018\)](#) describe the enormous lengths the EDGES team have gone to in order to minimize the errors in calibration and to account for the chromaticity, but it nevertheless seems likely that there are errors remaining which have the broad smooth structure needed to account for these effects. This is consistent with the fact that there are residuals of order 1 K peak-to-peak present when only 3rd or 4th order polynomials are fitted but that these drop to ~ 0.2 K peak-to-peak when a 5th order term is introduced.

The apparent detection of an absorption profile depends on the presence of “sharp” features in the spectrum, i.e. the structures with widths of ~ 5 to ~ 10 MHz seen in the residuals when the polynomials have been fitted, i.e., the top panels in the figures above. The concern is that if there are substantial systematic errors on these broad scales how can we be confident that these much lower-level narrow structures are not also due to systematic errors. [Bowman et al. \(2018\)](#) list the numerous tests that they performed which demonstrate that the features are present with different experimental setups, orientations of the antenna and when there are very different contributions to the signal from the galactic emission and other radio sources. They also report tests of the receiver and the calibration system that appear to rule those out as causes of structure of this sort at the level detected. As demonstrated above, however, the presence of a spurious ripple in data with an amplitude of only ~ 0.05 K, together with broader structures which can be removed by fitting a sixth-order polynomial, would provide a good fit without the need to invoke a ~ 0.5 K deep absorption feature.

3. CONCLUSIONS

We have analyzed the single released EDGES data set and have focussed on the issue of the fitting of the data. The data do clearly contain structure that is not consistent with the smooth shape expected for foreground emission. We confirm that it is consistent with the presence of the absorption profile described by [Bowman et al. \(2018\)](#) when a 5-term foreground model is fit and subtracted. We find, however, that:

1. The modelling process used by [Bowman et al. \(2018\)](#) implies non-physical properties for the foregrounds.
2. If the parameters of the foregrounds are constrained to plausible values, the fit is poor and the residuals do not then suggest the presence of an absorption feature.
3. A good fit can be obtained if sufficiently high-order polynomials are used to model the smoothly varying features and an absorption feature is included. Relatively small

changes in the modelling process can, however, produce good fits which give markedly different results for the properties of the absorption profile.

4. Completely different descriptions of the data, which do not include an absorption feature at all, can also provide a good fit but would require that there are some low-level instrumental effects present that have somehow escaped detection by the very careful work of the EDGES team.

ACKNOWLEDGEMENTS

We thank the EDGES team for making their data publicly available and for helpful exchanges about their result. It is a pleasure to acknowledge useful discussions with Avery Broderick, Jens Chluba, Eloy de Lera Acedo, George Efstathiou, Martin Haehnelt, William Handley, Roberto Maiolino, Christoph Pfrommer, Jonathan Pritchard, Nima Razavi, Martin Rees, and Sander Weinreb. G.K. acknowledges support from ERC Advanced Grant 320596 ‘The Emergence of Structure During the Epoch of Reionization’. P.D.M. and E.P. acknowledge support from Senior Kavli Institute Fellowships at the University of Cambridge. P.D.M. also acknowledges support from the Netherlands organization for scientific research (NWO) VIDI grant (dossier 639.042.730).

4. SUPPLEMENTARY INFORMATION

We write the observed sky brightness as

$$T_{\text{Sk}} = (T_{\text{Bg}} - T_{21} + T_{\text{Fg}}) e^{-\tau_{\text{ion}}} + T_e (1 - e^{-\tau_{\text{ion}}}), \quad (1)$$

where T_{Bg} represents the background radiation, i.e., that arising from redshifts greater than that where the absorption is occurring, T_{21} is the absorption feature, T_{Fg} is the foreground radiation, τ_{ion} is the opacity of the ionosphere, and T_e is the opacity-weighted temperature of the electrons in the ionosphere. One would normally take $T_{\text{Bg}} = 2.725$ K although some possible explanations for a strong absorption feature require a higher background (Feng and Holder 2018). It appears that Bowman et al. (2018) omitted this term so we have done so too. This has little effect on the results: the amplitude of the trough and the residuals change by only 1.1% and -0.5% , respectively when we redo the analysis shown in Figure 1 with the CMB included.

We adopt the flattened Gaussian profile used by Bowman et al. (2018)

$$T_{21}(\nu) = -A \left(\frac{1 - e^{-\tau e^B}}{1 - e^{-\tau}} \right), \quad (2)$$

where

$$B = \frac{4(\nu - \nu_0)^2}{w^2} \log \left[-\frac{1}{\tau} \log \left(\frac{1 + e^{-\tau}}{2} \right) \right], \quad (3)$$

A is the amplitude and ν_0 is the central frequency, while the parameters w and τ describe the width and flattening of the profile, respectively.

Bernardi et al. (2015) use an expansion in $\log(\nu/\nu_c)$ to describe the frequency dependence of the synchrotron foreground emission around some central frequency ν_c , which we have set to 75 MHz in all the results given here.

$$\log T_{\text{Fg}}(\nu) = \sum_{n=0}^{N-1} d_n [\log(\nu/\nu_c)]^n \quad (4)$$

This reduces to

$$T_{\text{Fg}}(\nu) = b_0 \left(\frac{\nu}{\nu_c} \right)^{d_1 + d_2 \log(\nu/\nu_c) + d_3 [\log(\nu/\nu_c)]^2 + \dots}, \quad (5)$$

where $b_0 = \exp(d_0)$ is the foreground brightness temperature at ν_c . If we assume that the opacity of the ionosphere scales as ν^{-2} (Rogers et al. 2015) then we can write $\tau_{\text{ion}} = b_3(\nu/\nu_c)^{-2}$. Dropping the quadratic and higher terms in $\log(\nu/\nu_c)$ then gives, for the combined contributions of the synchrotron and ionosphere but without the absorption feature:

$$T_{\text{Sk}}(\nu) = b_0 \left(\frac{\nu}{\nu_c} \right)^{-2.5 + b_1 + b_2 \log(\nu/\nu_c)} e^{-b_3(\nu/\nu_c)^{-2}} + T_e \left(1 - e^{-b_3(\nu/\nu_c)^{-2}} \right), \quad (6)$$

where $b_1 = d_1 + 2.5$ and $b_2 = d_2$. We refer to the foreground model of Equation (6) as the physical foreground model, to distinguish it from models constructed out of arbitrary smooth basis functions. We used this for the fits shown in Figure 2. If the ionospheric optical depth is small then Equation (6) becomes

$$T_{\text{Sk}}(\nu) = b_0 \left(\frac{\nu}{\nu_c} \right)^{-2.5 + b_1 + b_2 \log(\nu/\nu_c)} e^{-b_3(\nu/\nu_c)^{-2}} + b_4 \left(\frac{\nu}{\nu_c} \right)^{-2}, \quad (7)$$

where $b_4 \approx b_3 T_e$. Note that the connection between the ionospheric emission and absorption via the electron temperature has been lost by using this form. This is the expression given for the ‘‘physically-motivated’’ model by Bowman et al. (2018) and we used it when fitting with unrestricted priors. The results of least-squares fitting, with and without the absorption feature are shown in the top two lines of Table 1.

Bowman et al. (2018) use a linearized form of Equation (6), by assuming b_1 , b_2 and $b_3 \ll 1$. This yields

$$T_{\text{Sk}}^{\text{lin}}(\nu) = a_0 \left(\frac{\nu}{\nu_c} \right)^{-2.5} + a_1 \left(\frac{\nu}{\nu_c} \right)^{-2.5} \log \left(\frac{\nu}{\nu_c} \right) + a_2 \left(\frac{\nu}{\nu_c} \right)^{-2.5} \left[\log \left(\frac{\nu}{\nu_c} \right) \right]^2 + a_3 \left(\frac{\nu}{\nu_c} \right)^{-4.5} + a_4 \left(\frac{\nu}{\nu_c} \right)^{-2}, \quad (8)$$

where the new parameters a_i are related to the b_i as $a_0 = b_0$, $a_1 = b_0 b_1$, $a_2 = b_0(b_1^2/2 + b_2)$, $a_3 = -b_0 b_3$, and $a_4 = b_4$ in the regime in which the linear approximation is valid. We used Equation (8) to perform the fits shown in Figure 1 which confirmed that our procedures

match those of [Bowman et al. \(2018\)](#). Specifically for the least-squares process we minimize

$$\Delta T^2(\nu) = \sum_i [T_{\text{data}}(\nu_i) - T_{Sk}(\nu_i) - T_{21}(\nu_i)]^2. \quad (9)$$

The parameter values we obtain using this linearized form are given in [Table 1](#). (Note that we cannot rule out the existence of additional local minima outside the prior assumed in our Bayesian analysis below.)

A more general way of treating foregrounds is to take the viewpoint that a foreground models should fit the smooth component of the observed spectrum. The remaining sharp features are then possibly the absorption signal. In this treatment, assigning physical meaning to foreground parameter values is more difficult, but the signal extraction is likely to be less biased. Such models can be constructed out of a variety of smooth basis functions, including the log-polynomial described earlier. [Bowman et al. \(2018\)](#) used the polynomial form

$$T_{\text{Fg}}^{\text{poly}}(\nu) = \sum_{n=0}^{N-1} a_n \left(\frac{\nu}{\nu_c} \right)^{-2.5+n}, \quad (10)$$

with various values of N . We used this form to obtain the results shown in [Figure 3](#) and the corresponding parameter values are in the lower part of [Table 1](#).

We can explore the covariances between the parameter by obtaining their joint posterior probability distribution in Bayesian fashion. The posterior distribution is given by

$$p(\theta|d) = \frac{p(\theta)p(d|\theta)}{p(d)}, \quad (11)$$

where θ represents the model parameters, and d represents the data. The likelihood is given by $p(d|\theta)$, and $p(\theta)$ is the prior distribution. The quantity $p(d)$, given by

$$\mathcal{Z} \equiv p(d) = \int p(d|\theta)p(\theta)d\theta, \quad (12)$$

presents the evidence. We assume a Gaussian likelihood for the EDGES data, given a model including the foregrounds and, optionally, the flattened Gaussian absorption profile. The logarithm of the likelihood is given by

$$\log \mathcal{L} = \sum_i \left[-\frac{1}{2} \log(2\pi\sigma^2) - \frac{1}{2} \left(\frac{T_{\text{data}}(\nu_i) - T_{\text{model}}(\nu_i)}{\sigma} \right)^2 \right] \quad (13)$$

To sample the likelihood we used the nested sampler PolyChord ([Handley et al. 2015](#); [Handley et al. 2015](#)). We used $N_{\text{live}} = 2048$ live points, and ran PolyChord in parallel on 256 CPUs. For each run, depending on the number of degrees of freedom, results were derived within 30–90 minutes wall-clock time. We assumed a log prior for the σ parameter in [Equation 13](#) to vary $\in [10^{-1}, 10^{-4}]$ K, in addition to using assuming a fixed $\sigma = 10^{-2}$ K. Besides slightly slower convergence when varying σ , results were consistent. We typically

find $\sigma_{\text{best-fit}} \simeq 10^{-1.6}$. In all runs, we assume uniform priors on the absorption profile parameters with $A \in [0, 20]$, $\tau \in [0, 100]$, $\nu_0 \in [60, 90]$ and $w \in [1, 40]$. For the foreground parameters, we begin by choosing wide priors around the best-fit values obtained from the least-squares optimization: $b_0 \in [1, 10000]$, $b_1 \in [-10, 10]$, $b_2 \in [-10, 10]$, $b_3 \in [-10, 10]$ and $b_4 \in [-10000, 10000]$. The resulting posterior distribution is shown in Figure 5. The posterior median values are consistent with the best-fit values obtained from the least-squares optimization. Figure 6 shows the posterior distribution when the foreground parameters are restricted to physical values, i.e., $b_0 \in [10, 100000]$, $b_1 \in [-2, 0]$, $b_2 \in [-0.1, 0.1]$, $b_3 \in [0.005, 0.2]$ and $T_e \in [200, 2000]$ K as explained above. It is clear from the posteriors that our restricted priors limit the fitting of an absorption line consistent with that of a 21-cm signal from the cosmic dawn. Specifically b_3 prefers to be negative, which, as explained, is unphysical. Furthermore, if any absorption profile, its central frequency prefers to be $\nu > 90$ MHz. For the 5-term polynomial foreground model of Equation (10) we used uniform priors for $a_i \in [-20000, 20000]$. If we do not restrict the frequency range, we cannot recover the best-fit feature obtained with the physical model and the linearized version. We compare the posteriors on the absorption profile parameters in Figure 7. We show results for both the full frequency range and the restricted frequency range including foreground parameters in Figure 8 and Figure 9 respectively. Of all models considered (including several models not discussed here) the polynomial foreground model fit, over the full frequency range, was the most likely model, based on Bayesian evidence ratios, as seen in Table 1.

REFERENCES

- G. Bernardi, M. McQuinn, and L. J. Greenhill. “Foreground model and antenna calibration errors in the measurement of the sky-averaged 21 cm signal at $z \sim 20$.” *The Astrophysical Journal*, 799(1):90, 2015.
- J.D. Bowman, A.E.E. Rogers, R.A. Monsalve, T.J. Mozdzen, and N. Mahesh. “An absorption profile centred at 78 megahertz in the sky-averaged spectrum.” *Nature*, 555(7694):67–70, 2018.
- J. V. Evans and T. Hagfors. “Radar astronomy.” New York: McGraw-Hill, 1968.
- C. Feng and G. Holder. “Enhanced global signal of neutral hydrogen due to excess radiation at cosmic dawn.” arXiv:1802.07432 [astro-ph.CO]
- W. J. Handley, M. P. Hobson, and A. N. Lasenby. “POLYCHORD: next-generation nested sampling.” *MNRAS*, 453:4384–4398, November 2015.
- W. J. Handley, M. P. Hobson, and A. N. Lasenby. “PolyChord: nested sampling for cosmology”. *Mon. Not. Roy. Astron. Soc.*, 450(1):L61–L65, 2015.
- T. J. Mozdzen, J. D. Bowman, R. A. Monsalve, and A. E. E. Rogers. “Limits on foreground subtraction from chromatic beam effects in global redshifted 21 cm measurements.” *MNRAS*, 455:3890–3900, February 2016.
- A.E.E. Rogers, J. D. Bowman, J. Vierinen, R. Monsalve, and T. Mozdzen. “Radiometric measurements of electron temperature and opacity of ionospheric perturbations.” *Radio Science*, 50(2):130–137, 2015.

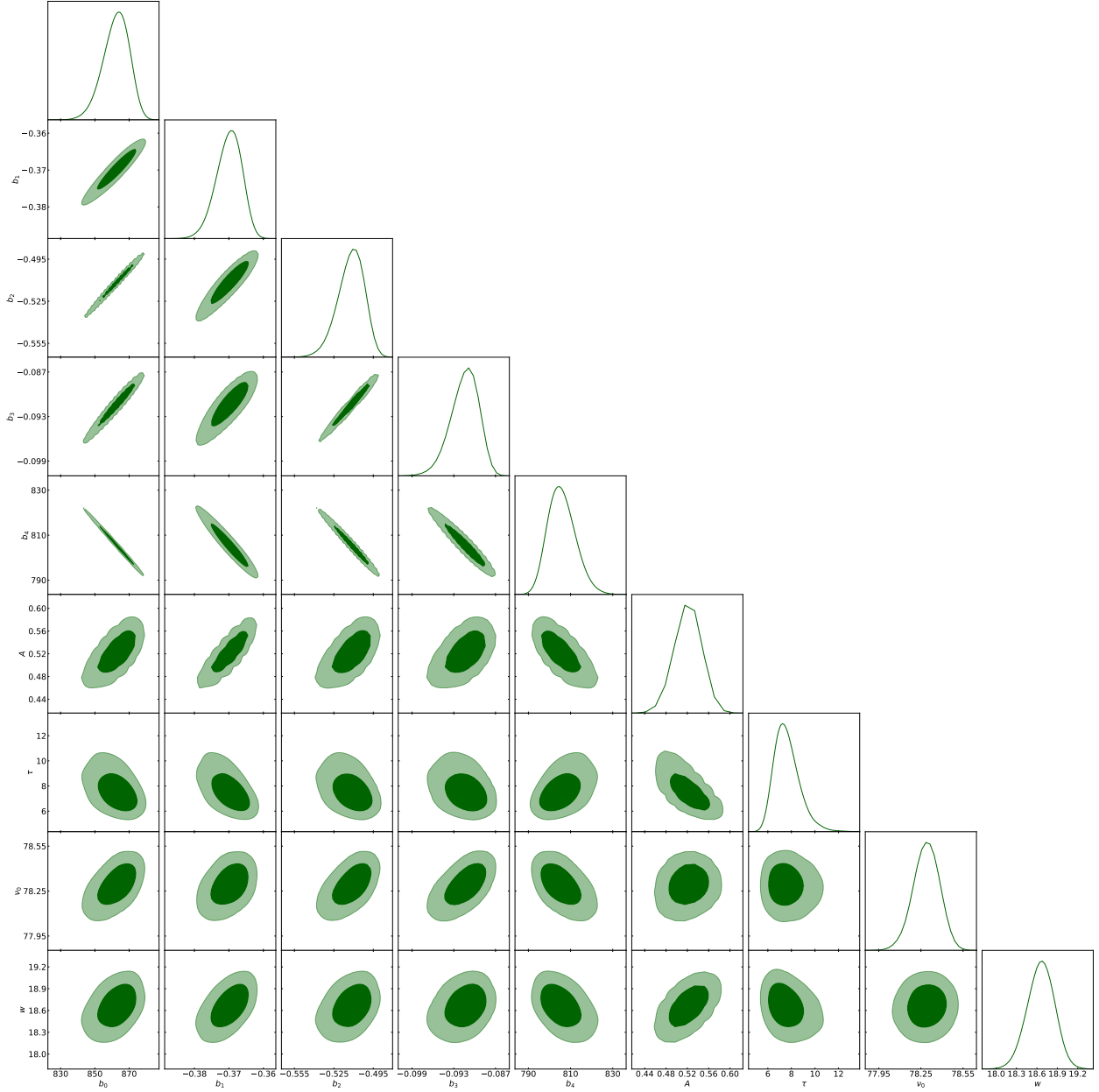


Figure 5. Parameter posterior distributions when the physical foreground model from Equation (6) is fit to the EDGES data with the flattened Gaussian absorption profile, using broad priors on the parameter values. We obtain results on the feature parameters that are consistent with Bowman et al. (2018).

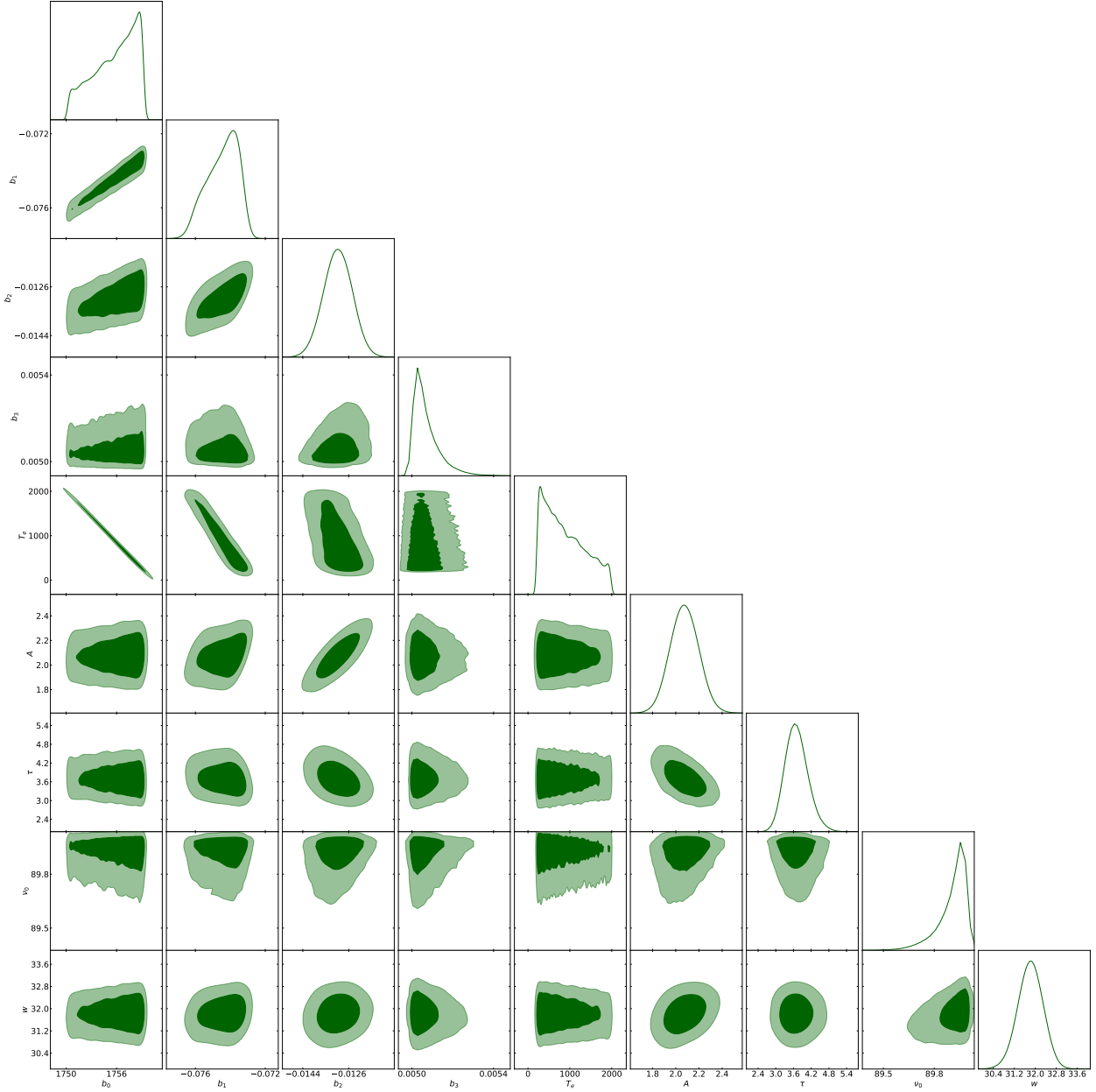


Figure 6. Same as Figure 5 but with priors on the foreground parameters restricted to span physically plausible values. Restraining the foregrounds does not provide a good fit, as foregrounds prefer values outside the prior range. In the above we set a prior on the central frequency of the absorption profile of $60 \leq \nu_0 \leq 90$, and the data prefers a feature $\nu_0 > 90$ with a absorption depth $A > 2$ K. Also note that we have associated the b_3 and b_4 with the ionosphere and our last foreground parameter is now T_e .

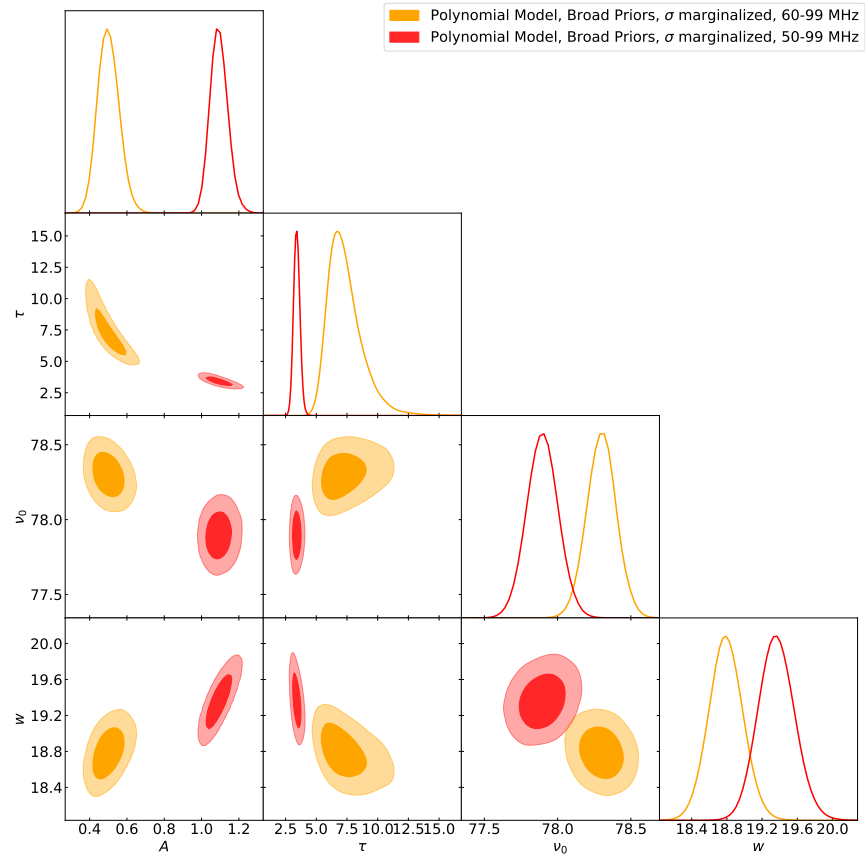


Figure 7. Marginalized posterior probability distribution for the flattened Gaussian absorption profile parameters in the polynomial foreground model case, when the model is fitted to the full EDGES data (red) and when it is fitted to a subset of the data (orange). When the full data are considered, the preferred absorption-line profile has an amplitude of 1 K. The result of [Bowman et al. \(2018\)](#) is recovered only when the analysis is restricted to a subset of the data.

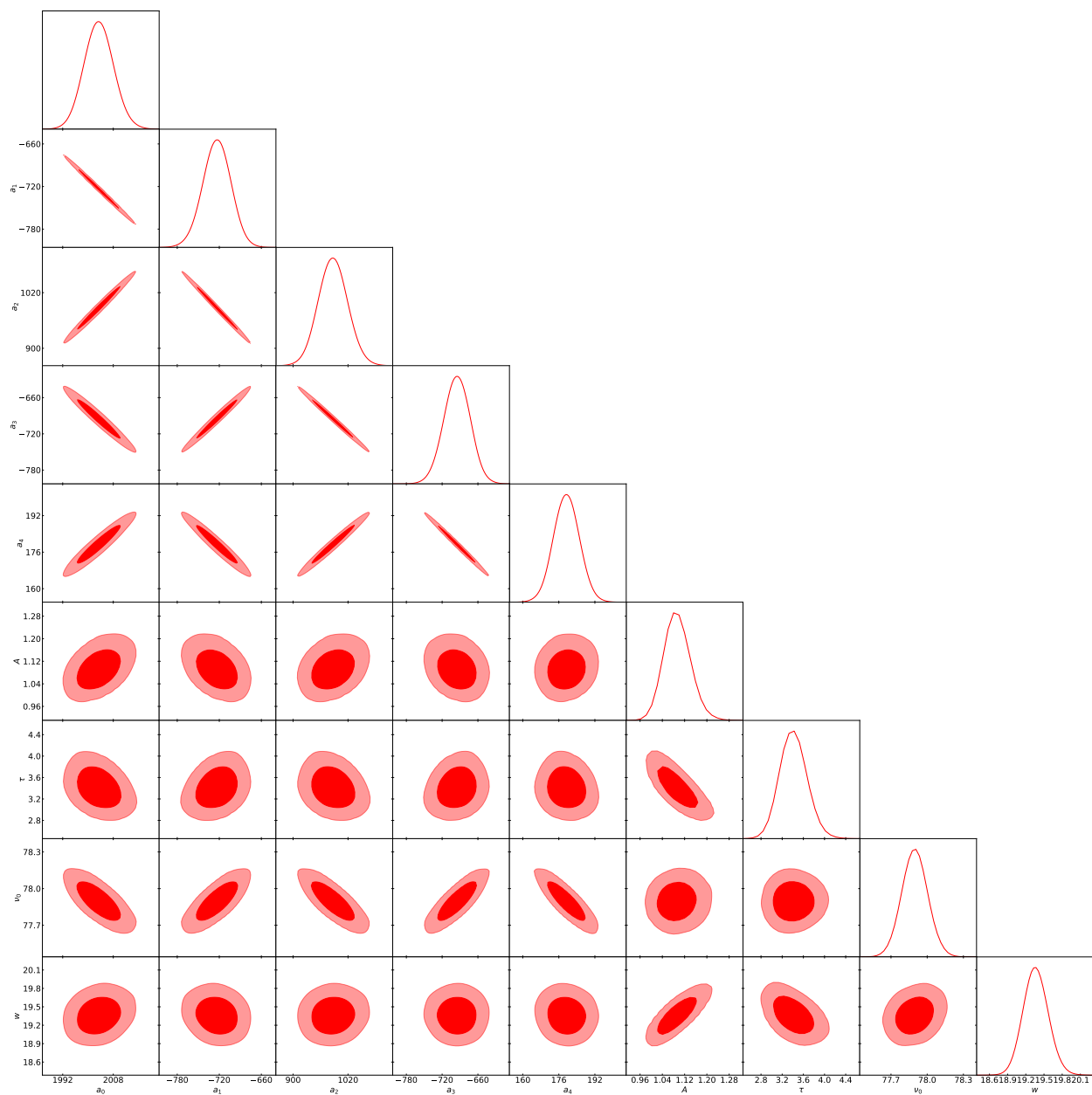


Figure 8. Parameter posterior distributions when the polynomial foreground model is fitted to the full EDGES data.

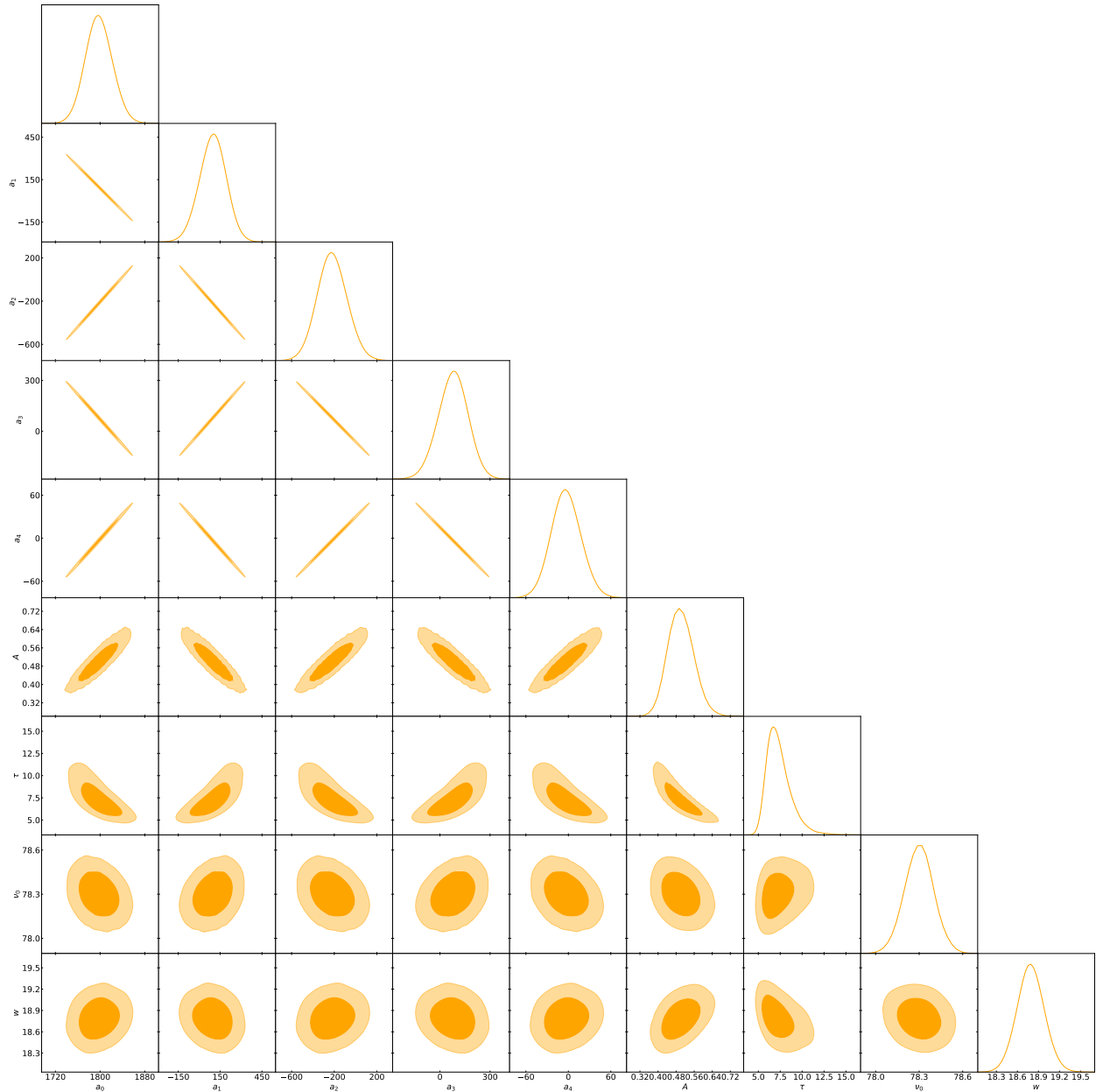


Figure 9. Parameter posterior distributions when the polynomial foreground model is fitted to the restricted EDGES data in the range 60–99 MHz. We expected these results to match those shown in Extended Data Figure 10 of [Bowman et al. \(2018\)](#). The parameters for the profile are similar but we find very different values for the polynomial terms.

Table 1. Best-fit parameter values of the least-square fits of all models discussed in the text.

Physical foreground model												
b_0	b_1	b_2	b_3	b_4	A	τ	ν_0	w	residual rms	$\log \mathcal{Z}$		
739.947	-0.43953	-0.69457	-0.12488	911.904					0.084	6.4 ± 0.3		
870.236	-0.36629	-0.50181	-0.089482	799.045	0.540	6.97	78.34	18.74	0.024	194.6 ± 0.2		
Physical foreground model (restricted priors) ^a												
b_0	b_1	b_2	b_3	T_e	A	τ	ν_0	w	residual rms	$\log \mathcal{Z}$		
1753.466	-0.080185	-0.021731	0.0052115	1135.896					0.235	16.7 ± 0.3		
1755.753	-0.074443	-0.013026	0.0050689	894.275	2.075	3.71	89.91	31.81	0.122	-215.1 ± 0.2		
Linearised physical model												
a_0	a_1	a_2	a_3	a_4	A	τ	ν_0	w	residual rms	$\log \mathcal{Z}$		
-15431.048	-8213.422	-2582.357	199.642	16981.681					0.088	69.0 ± 0.2		
-10111.419	-5673.739	-1831.621	150.673	11711.500	0.553	6.78	78.31	18.74	0.024	202.0 ± 0.2		
$N = 5$ polynomial model												
a_0	a_1	a_2	a_3	a_4	A	τ	ν_0	w	residual rms	$\log \mathcal{Z}$		
1923.462	-411.123	552.437	-443.101	128.646					0.140	-		
2003.457	-723.697	987.515	-695.483	179.496	1.091	3.41	77.90	19.35	0.025	203.7 ± 0.3		
$N = 5$ polynomial model fitted to 60–99 MHz												
a_0	a_1	a_2	a_3	a_4	A	τ	ν_0	w	residual rms	$\log \mathcal{Z}$		
1525.901	1169.801	-1781.394	1072.851	-236.985					0.041	-		
1802.667	78.025	-191.409	60.397	1.029	0.511	6.88	78.29	18.80	0.018	192.2 ± 0.2		
$N = 6$ polynomial model												
a_0	a_1	a_2	a_3	a_4	a_5				residual rms	$\log \mathcal{Z}$		
2670.795	-4440.963	9139.282	-9479.983	4826.027	-964.945				0.046	26.0 ± 0.2		
$N = 6$ polynomial model + sinusoidal ($T_{\text{line}} = A \sin(2\pi\nu/l + \phi)$)												
a_0	a_1	a_2	a_3	a_4	a_5	A	ϕ	l	residual rms	$\log \mathcal{Z}$		
2625.771	-4202.081	8636.317	-8954.631	4553.795	-908.957	0.057	5.74	12.27	0.026			

^aNote that for the cases with a restricted prior the mean values of the posterior rather than least-square fit parameters are given.